ISSN 0967-859X
THE SOCIETY FOR EARTHQUAKE AND
CIVIL ENGINEERING DYNAMICS

NEWSLETTER

Volume 23 No 1
June 2011

In this issue

Performance Based Earthquake Damage Assessment

&

Development of Dissipative Retrofitting Devices for Masonry Buildings

Dina D'Ayala
University of Bath

Sara Paganoni
University of Bath

Introduction

The earthquake that occurred in L'Aquila, Abruzzo, in April 2009, was extremely damaging to the historic centres of the Region. Almost two years later most of the heritage buildings in the historic city centre of L'Aquila, whether major monuments or ordinary residential buildings, are still far from having been repaired, and the heart of the city looks more like a ghost town than the thriving commercial and cultural centre home to 70000 people that it used to be on the eve of April 6th 2009.

Following the earthquake the authors carried out two campaigns of survey with the aim of recording the damage to historic buildings, evaluate their vulnerability and validate a performance based approach to the development of fragility curves for this class of structures using the FaMIVE method (D'Ayala and Speranza, 2003), whereby feasible collapse mechanisms and the associated failure load factors can be identified.

One of the aims of this activity is to collect evidence and quantitative data that would guide the design and calibration of dissipative retrofitting devices, tailored for heritage buildings, which would increase their resilience in future events. The methodology followed to develop and validate the dissipative devices is presented in the second part of the paper.

The presence in literature of procedures for displacement-based vulnerability assessment of historic masonry is modest. Among the methods available, the ones based on mechanism identification are particularly suitable for use within displacement-based performance assessment (Lang and Bachmann, 2004; D'Ayala, 2005; D'Ayala et al., 2008; Lagomarsino and Giovinazzi, 2006; Crowley et al., 2004; Bernardini and Lagomarsino, 2008). These models associate capacity curves with specific construction characteristics or building typologies, which can be consid-

ered as having a homogeneous response to seismic hazard. Capacity curves are usually defined assuming either in-plane or out-of-plane failure behaviour and quantifying strength and displacement by computing simple geometric parameters (cross sectional area of walls at chosen levels, inter-storey height, etc.) and few mechanical parameters (characteristic shear strength or coefficient of friction and compression strength) inferred on the basis of knowledge of the materials or by limited testing. The definition of the capacity curve of specific limit states (corresponding to predefined displacement values) and correlation of these to damage states eventually allows definition of the distribution of different damage levels over a population of buildings, a mean damage value and standard deviation, and hence the derivation of fragility curves for different levels of shaking. One of the advantages of such an approach is that since it allows evaluating the capacity of the structure as an analytical function of a modest number of geometrical and mechanical parameters, it is possible to apply suitable procedures for the propagation of uncertainty. A robust analytical procedure needs extensive validation by correlating its damage estimates with observed earthquake damage data, and verifying that the chosen parameters are representative of the building stock, both in terms of hypothesis of structural behaviour (flexible versus rigid horizontal structures, out-of-plane versus in-plane resisting mechanism, etc.) and actual numerical values.

The use of a procedure proposed by D'Ayala (2005) is presented here to analyse the earthquake effects on the historic centre of L'Aquila. It uses limit state analysis with a mechanism approach to obtain realistic pushover curves for structural masonry components and has been coded within the FaMIVE procedure (D'Ayala and Speranza, 2003). The procedure has been validated with empirical data from various seismic events and applied to define risk scenarios in Europe and Asia (Bernardini et al., 2008; D'Ayala and Ansal, 2009).

Sample characterisation and damage observation

The damage observed in L'Aquila is classified using the mechanism catalogue developed for the FaMIVE procedure (D'Ayala and Speranza, 2002), to establish correlation between construction details and damage types from visual inspection of a larger number of buildings. The partial or total overturning of the façade is due to poor quality of connections between walls or parts of them (Figure 1). When the quality of the masonry fabric at the corners is enhanced by the presence of quoins, the façade is not allowed to overturn and mechanism types B or C will preferably develop (Figure 2). The occurrence of either type depends on opening layout; spanning direction of the horizontal structures; presence of internal load bearing walls normal and connected to the façade. When out-of-plane mechanisms of the types described above are prevented by efficient connections among orthogonal walls then in-plane mechanisms, mainly activating the shear capacity of the masonry, are likely to develop. The occurrence of regular diagonal X shaped cracks in the spandrels or piers is not the most common case. This is due to various issues: the irregular distribution and size of opening leads to an un-

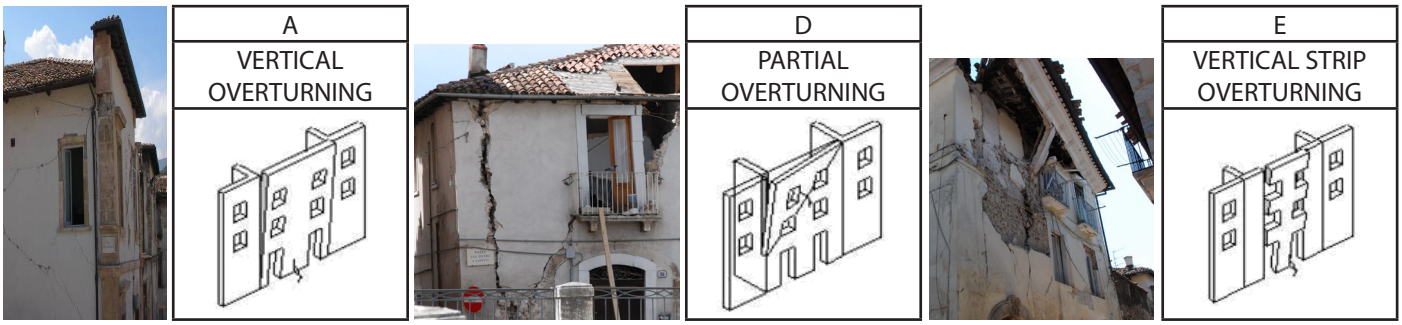

Figure 1. Out-of-plane mechanisms due to poor connections at corners: damage mechanism A, complete overturning of façade; damage mechanism D, partial overturning along a diagonal; mechanism E, partial overturning of the openings vertical strips

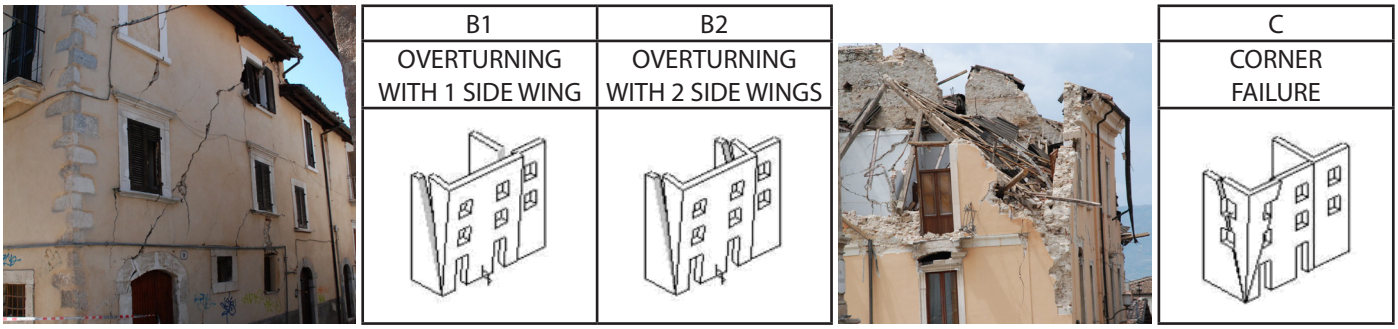

Figure 2. Effect of good connections at corners: damage mechanism B, overturning with side wing/s (left); damage mechanism C, corner failure (right)

even distribution of stiffness and shear capacity among the piers; or the flexibility of the floor structures.

Furthermore the piers might be failing in a combination of bending and shear, rather than just shear (Casapulla and D'Ayala 2006). For these reasons mechanisms H and H2 depicted in Figure 3 are calculated by identifying the weakest load path in the façade leading to shear failure, rather than simply using lateral capacity of the piers and assuming a rigid behaviour of the spandrel. Cross-ties, which originally might have been introduced to counteract the trust generated by vaults, also help to protect the façades from out-of-plane damage in a large number of cases. When the façade is prevented from moving out at the roof level and along the edges, it might behave like a constrained plate, with out-of plane movement at a lower level. When the mechanism fully develops is identifiable by the bowing out of the walls (Figure 4). For the restraints to be effective the ties should be regularly spaced over the façade and correctly anchored and connected through to the orthogonal walls or to the floor structure. When this is not the case, and the unrestrained length of the façade is considerable in respect to its thickness, then mechanisms of type G are likely to occur.

The location of surveyed buildings is recorded on the map of Figure 5, together with the maximum level of damage and prevalent failure mechanism observed for each façade. An almost equal proportion of buildings shows a maximum level of damage 2 (28%), 3 (32%) or 4 (26%), with a minority showing damage 0-1 (5 %) or 5 (6%). The sample has been divided in five categories classified by masonry and floor structure type: brickwork with flexible horizontal structures (UFB3) or with stiffer horizontal structures (UFB5), dressed stone with flexible (DS2) or stiffer (DS4) horizontal structures, and poorly dressed and rubble stonework (RS3).

The FaMIVE procedure calculates the most likely mechanism to occur for a given façade or elevation, with given connections to the rest of the structure, using a limit state analysis and lower bound approach. The procedure calculates first the collapse load factor associated with each possible mechanism for a wall, i.e. the mechanisms that can develop given the constraint conditions surveyed (as given in Figure 1 to Figure 4), then chooses the "worst" in terms of the highest result of the product between the inverse of the collapse load factor and the damage extent.

The diagram in Figure 6 shows the number of façades or elevations in each structure type, subdivided in in-plane or out-of-plane mechanism, on the basis of the analysis' results. The majority of buildings are either made of poorly dressed stone (RS3, 42% of the sample) or dressed stone with either timber floors (DS2, 21%) or steel joist and tiles (DS4, 5%). A third of the building stock surveyed, usually of recent construction, is made of brick work with timber floors or concrete slabs (UFB, 31%). According to the assessment, the majority of the stone masonry buildings fail in an out-of-plane mechanism, while the brickwork buildings have a majority of in-plane failures. As stated in the general description of damage in the previous section, the occurrence of out-of-plane failure is hindered or prevented by presence of quoins or ties, if these are well distributed.

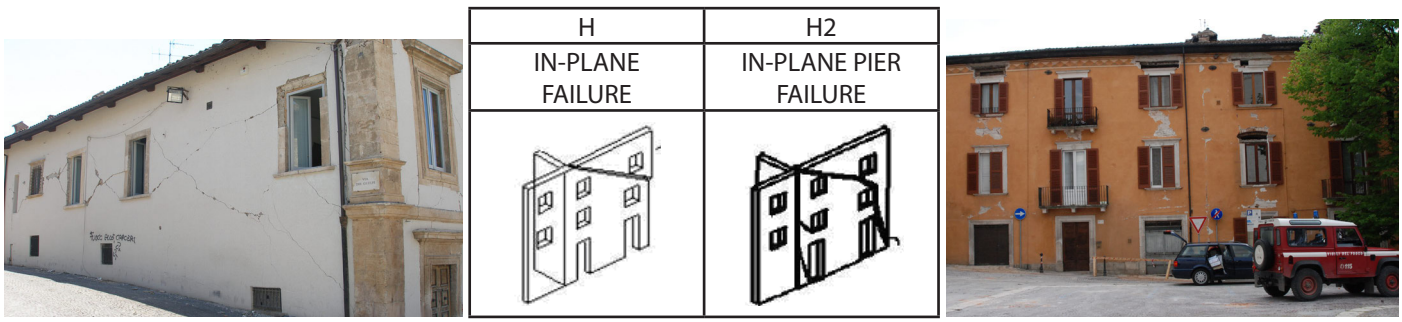

Figure 3. In-plane damage mechanism in pier, H (left); and combined in piers and spandrels, H2 (right)

Figure 4. Damage mechanism F, vertical arch (left); and damage mechanism G, horizontal arch (right)

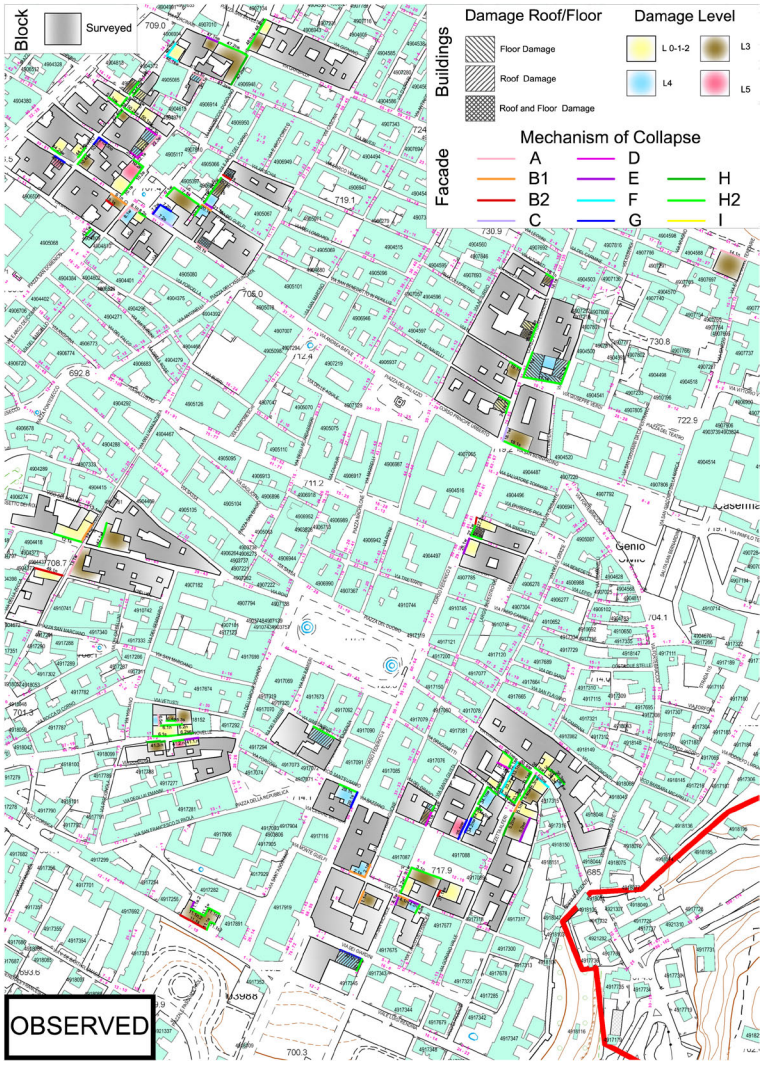

Figure 5. Localisation of the surveyed sample within the historic city centre of L'Aquila. Mapping of observed damage levels and collapse mechanisms of the façades.

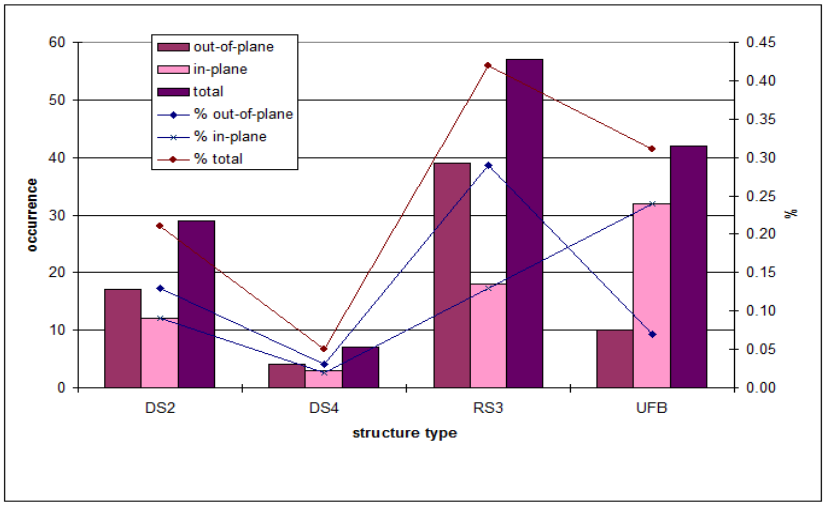

Figure 6: Distribution of structures types (RS3, DS2, DS4, UFB) and associated in-plane and out-of plane failure modes by façades, within the sample of 90 buildings surveyed with the FaMIVE procedure. For each building typically one or two façades are analysed, depending on access

Definition of capacity curves and identification of performance points

Besides calculating the ultimate lateral capacity associated with the most vulnerable mechanism, in order to assess and predict levels of damage given a specific ground motion, it is essential to define capacity curves. In the present study, on the basis of the observations on site, average capacity curves are developed for each of the building classes identified above. The theoretical background to this approach is presented in D'Ayala (2005). The procedure adopted is summarised in the following. The first step is to calculate the lateral effective stiffness for each wall and its tributary mass. The effective stiffness for a wall is calculated on the basis of the type of mechanism attained, the geometry of the wall and layout of openings, the constraints to other walls and floors and the portion of other walls involved in the mechanism:

$$K_{\text{eff}} = k_1 \frac{E_t I_{\text{eff}}}{H_{\text{eff}}^3} + k_2 \frac{E_t A_{\text{eff}}}{H_{\text{eff}}} \qquad (1)$$

where H_{eff} is the height of the portion involved in the mechanism, E_t is the estimated modulus of the masonry as it can be obtained from experimental literature, I_{eff} and A_{eff} are the second moment of area and the cross sectional area, calculated taking into account extent and position of openings and variation of thickness over height, k_1 and k_2 are constants which assume different values depending on edge constraints and whether shear and flexural stiffness are relevant for the specific mechanism.

The tributary mass is calculated following the same approach, and it is equal to the volume of the extent of the wall times the masonry density plus the mass of the horizontal structures involved in the mechanism. The effective mass and effective stiffness are used to calculate a natural period, for an equivalent single degree of freedom oscillator. The mass is applied at the height of the centre of gravity of the collapsing portion, with respect to the ground, and a constant acceleration distribution over the wall height is assumed. For out-of-plane mechanisms the acceleration and displacement values defining the elastic limit, can be computed as follows. The elastic limit acceleration A_y is identified as the combination of lateral and gravitational load that will cause a triangular distribution of compression stresses at the base of the overturning portion, just before the onset of partialisation. This can be calculated as:

$$A_y = \frac{t_b}{6h_0} g \qquad (2a)$$

with corresponding displacement

$$\Delta_y = \frac{A_y}{4\pi^2} T^2 \qquad (2b)$$

where t_b is the effective thickness of the wall at the base of the overturning portion, h_0 is the height of the overturning portion, and T the natural period of the equivalent SDF oscillator. For in-plane mechanisms a similar equation is applied assuming a compressive strut in each pier with t_b and h_0 equal to the width of the strut and the inter storey height respectively. The next point on the pushover curve corresponds to the conditions of maximum lateral capacity A_u:

$$A_u = \frac{\lambda_c}{\alpha_1} g \qquad (3)$$

where λ_c is the load factor of the collapse mechanism chosen, calculated by FaMIVE, and α_1 is the proportion of total mass participating in the mechanism. This is calculated as the ratio of the total mass of the façade and sides or internal walls and floors involved in the mechanism. The corresponding displacement at incipient collapse is identified by the condition of loss of vertical equilibrium which, for overturning mechanisms, can be computed as a lateral displacement of the top of the wall

$$D_u = \frac{t_b}{3} \qquad (4)$$

with t_b wall thickness at the base of the overturning portion.

An intermediate point between (D_y, A_y) and (D_u, A_u) can also be identified, which corresponds to the position of the resultant of stresses for the fully partialised cross section at the base. If a parabolic stress block is assumed, the corresponding relative displacement of the top to the base is $D_{sd} \approx t_b/6$. This results in a value of ductility $\mu = D_u/D_{sd} = 2$, and is conceptually equivalent to defining a q factor.

The 3 points identified can be associated with corresponding states of damage as proposed in Figure 7 where the linearised and normalised curves for each structure type groups are presented. For each curve, DL (damage limitation) corresponds to the elastic lateral capacity (D_y, A_y), SD (significant damage) corresponds to the peak capacity (D_{sd}, A_u) and NC (near collapse) corresponds to incipient or partial collapse (D_u, A_u). In Figure 7 a point Δc is also identified corresponding to the displacement causing total collapse. It is noticeable that the DS4 group shows the higher stiffness and capacity, while DS2 has highest ductility, but lowest peak capacity. The rubble stone group is characterised by an almost linear behaviour up to maximum capacity and a very modest post peak ductile range.

In Figure 8 the average capacity curves are compared with the EC8 acceleration displacement response spectra (ADRS) having assumed a soil type B and the ADRS obtained from the strong ground motion record closer to the city, AQK (download of the corrected time histories from http://itaca.mi.ingv.it/ItacaNet/, last accessed 20/04/2010). For both cases, besides the linear spectra also the non-linear spectra obtained for a ductility μ = 2 are shown in Figure 8, this being the level of ductility calculated from the capacity curves. It should be noted that when compared with the non-linear EC8 spectrum the performance point for UFB3, DS2 and DS4 falls in the range between SD and NC, while for RS3 the curve falls short of it. With respect to the non-linear spectrum obtained from the record AQK longitudinal component, the situation is slightly more complex, but indicates that, apart from the DS4 type, the other three structure types would all have experienced substantial structural damage. It is worth noting however that the curves shown are affected by the uncertainty associated with the modelling, plus the uncertainty associated with the data collection. This is evaluated in terms of reliability of the data for each subsection of the form and is classified as high, medium and low, depending on whether specific data could be measured on site or on drawings, inspected

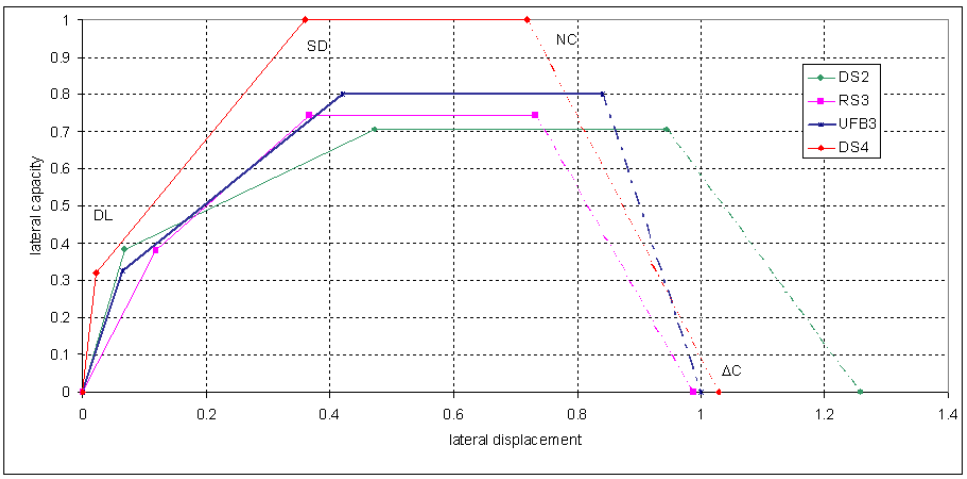

Figure 7: Normalised and linearised average capacity curves for each of the structure types in L'Aquila city centre

on site, or attributed by photo documentation respectively. In Figure 8 for each structure type capacity curve, the range of minimum and maximum values of accelerations is also marked for each damage point. The ranges show that only the best performing of buildings DS4 would be able to survive the earthquake within the threshold of structural damage, while the other structural types even at their best performance would have to rely on ductility and hence extensive cracking to survive the earthquake. This shows good correlation with the proportion of maximum observed damage levels reported in the previous section.

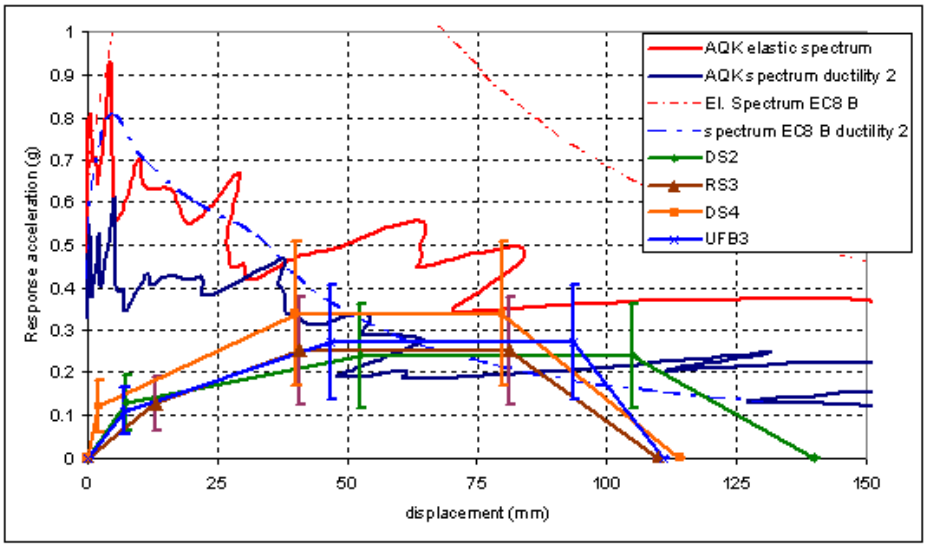

Figure 8. Comparison of capacity curves for each structure type, including uncertainty range, with the EC8 linear response spectrum for soil type B; the nonlinear response spectra obtained from this by using a ductility μ = 2; the response displacement elastic spectrum for record AQK longitudinal component; the corresponding non-linear spectra obtained for the same value of ductility. The non-linear spectra have been derived using Seismosignal ©.

Correlation between observed and computed mechanisms and level of damage

In order to assess how realistic the capacity curves and performance points obtained for the L'Aquila samples are, a comparison is drawn between observed and computed mechanisms and between relative position of NC collapse point and performance target, and observed damage.

To carry out this correlation the following assumptions have been made and summarised in Table 1. During the on-site survey up to three mechanisms might be associated with a given crack pattern or might be coexisting on the same wall, typically a prevalent, a secondary or possible, and/or a local mechanism (for instance overturning of the upper spandrel and in-plane failure, etc.). For the FaMIVE procedure output, up to two possibilities are considered, corresponding to the instance that two mechanisms have very similar collapse load factors and pertain to the same vulnerability class. With these assumptions, a score of 1 is given to the correlation if the first FaMIVE choice matches the prevalent mechanism observed, a score of 2 if it matches the secondary mechanism, and a score of 3 if it matches the local mechanism. If the FaMIVE second choice matches any of the observed mechanisms a score of 4 is given. Finally if there is no matching a score of -1 is given.

Table 1 shows that the prevalent mechanism is correctly predicted in 50% of cases and the alternative second worst in 27% of cases, while possible and local mechanisms represent a minority, and no correct prediction represent 9% of cases. The results show that there is high correspondence between the basic out-of-plane mechanism and the damage level and the capacity of the programme to predict it correctly. For the in-plane mechanisms H and H2, which account for almost 50% of the sample, the correlation is good.

A sample of the calculated mechanisms and vulnerability levels is evenly shared between medium level vulnerability (45%) and high level vulnerability (48%). A small minority have extreme vulnerability (4.5%) or low vulnerability (2.5%) These values correspond well in statistical terms with the observed level of damage shown in Figure 5, although with a slight shift towards a more vulnerable scenario than actually observed as highlighted in Table 2.

As far as the damage is concerned the comparison is carried out by looking at the level of damage observed against the predicted position of the performance point with respect to the near collapse point for the acceleration-displacement EC8 response spectrum with ductility μ = 2. It is then seen that while most of the UFB and DS4 representative NC points are to the right of the target performance point, for rubble buildings these mostly lie on the left, predicting collapse. As the number of collapses observed is definitely smaller than that computed the data is further analysed to quantify the error, as shown in Table 2.

Results can also be presented in terms of fragility curves (Figure 9) to provide guidance for future earthquake scenarios and retrofitting decision making. It can be seen that the greater standard deviation and ductility of the structure type DS2 clearly results in a less steep fragility curve especially at collapse. The poor performance of rubble masonry is also clearly highlighted at collapse. However for the limit state of structural damage the difference between RS3, DS4 and UFB3, is modest.

Observed mechanism	Criterion	Predicted Mechanism	Identification Score	Occurrence (%)
Prevalent mechanism	=	FaMIVE first choice	1	50
Possible mechanism	=	FaMIVE first choice	2	12
Local mechanism	=	FaMIVE first choice	3	2
Any of the above	=	Alternative second choice	4	27
Any of the above	≠	Any of the above	-1	9

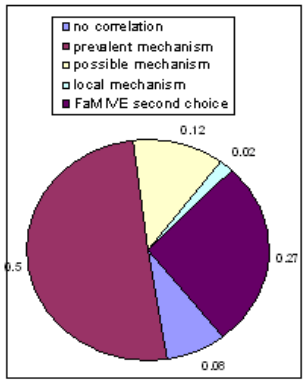

Correlation between observed and computed mechanisms

Table 1. Identification scoring criterion and occurrence

Structure type	Under-estimate 1 damage state	Correct	Over-estimate 1 damage state	Over-estimate 2 damage state	Over-estimate 3 damage state
DS2	0.10	0.21	0.24	0.28	0.17
DS4	0.14	0.43	0.14	0.28	0
RS3	0	0.25	0.35	0.30	0.10
UFB	0.05	0.27	0.32	0.32	0.04
Total	0.05	0.25	0.3	0.29	0.1

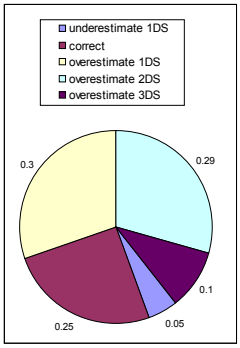

Table 2. Error in estimating the correct damage state for structure typology

Results of the survey confirmed that the presence of metallic cross-ties can be crucial to prevent out-of-plane failures of unreinforced masonry walls. This traditional system, which has been and still is commonly applied in rehabilitation practice all over Europe (Tomaževič, 1999), meets the requirement of restoring the box-like behaviour, allowing for the redistribution of horizontal load in sets of perpendicular walls without substantially increasing the mass. Ties indeed provide connection between perpendicular sets of walls, where poor quality, previous damage, or general wear and tear facilitate crack onset and eventual out-of-plane failure. Nonetheless, cross-ties can also cause pull-out damage at the head of the anchorage and increase in-plane diagonal cracking because of the different deformability of steel and masonry. This might become a major problem when damage limitation should be pursued avoiding cracking in precious plasters, frescoes, or other culturally valuable finishes. Drawing on these observations, the second part of the paper presents the development of an innovative typology of anchors: a dissipative device is installed in series with a grouted stainless steel anchor at the joint of perpendicular walls, where out-of-plane cracking is most likely to develop.

Rationale for the development of dissipative anchoring devices

Notwithstanding the consolidated assumption of performance-based design for new structures, current codes still acquiesce to the use of traditional stiffness-based techniques for the retrofit of historic buildings (EN 1998 Eurocode 8; Italian Ministry of Cultural Heritage and Activities, 2006). The application of techniques involving ductility and energy dissipation, despite being allowed in principle, is in fact limited since innovative systems rarely meet some of the constraints – reversibility, low impact – required for interventions on historic structures. Few high-profile case studies indeed appear in the literature (Indirli and Castellano, 2008; Benedetti, 2004; Mandara and Mazzolani, 1994).

However, strength-based techniques are unsuitable for historic low shear capacity masonry walls: L'Aquila earthquake, Italy, April 2009 proved once more that elements such as concrete ring beams, due to the elevated mass and stiffness, often aggravated by inadequate connections, do concur to cause tragic collapses (D'Ayala and Paganoni, 2011). Conversely, as shown in the previous sections, unreinforced masonry buildings benefit from the presence of cross-ties, despite some drawbacks related to the difference

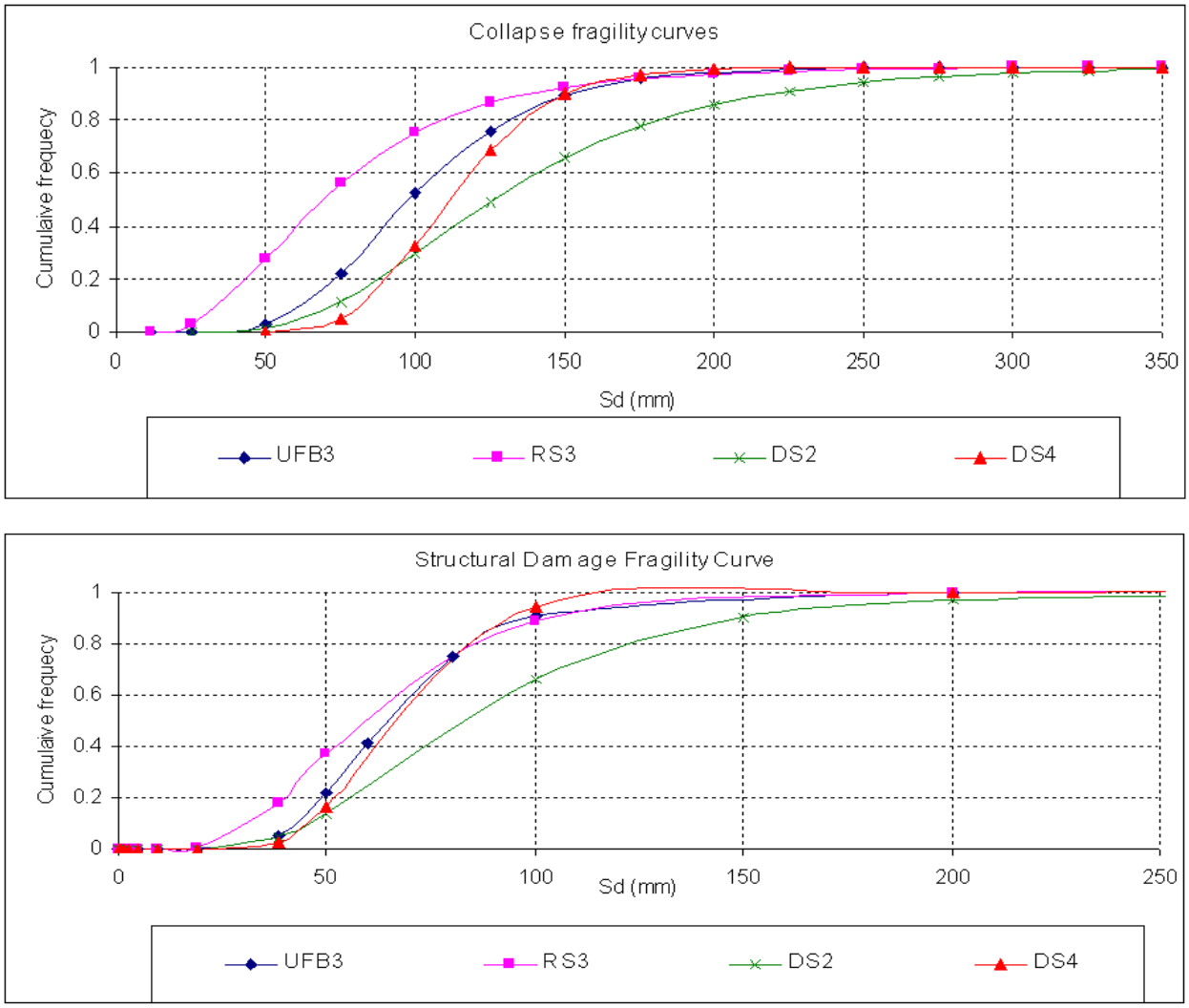

Figure 9: Fragility curves based on displacement at collapse

in stiffness between steel and parent material.

Drawing on the above observations, the authors developed, within the framework of a Knowledge Transfer Partnership (KTP) between the University of Bath and Cintec International Ltd, a dissipative device specifically designed to address the lack of passive systems for the seismic protection of heritage buildings.

The device is conceived as an add-on for Cintec's stainless steel ties and is designed to be placed at the locations where cracking is most likely to occur or is already present, so that in case of relative movements the devices can be activated. Thanks to either the hysteretic properties of a stainless steel element, shaped to optimise its post-elastic behaviour, or a friction mechanism set to be triggered for a certain level of pulling force, the device allows small relative displacements, dissipating energy and hence reducing the impact of seismic force on the walls, and controlling damage.

Initial experimental work, reported elsewhere (Paganoni and D'Ayala, 2009), included cyclic tests of the isolated devices over a range of frequencies relevant to the typical frequency content of European earthquakes. A target displacement of ±10 mm, comparable to the allowable interstorey drift required by current guidelines (OPCM 2005), was achieved, and the design of the devices was fine tuned so as to obtain stable and repeatable behaviour.

The paper presents the results of two experimental campaigns aiming to assess the performance of the dissipative anchoring devices embedded in low shear capacity masonry. The devices have also been modelled with a Finite Element (FE) package to simulate further scenarios; conclusions are drawn on the basis of the comparison between experimental and computational results.

Pull-out tests

The purpose of pull-out tests is to analyse the behaviour of the dissipative anchors in masonry panels with low shear capacity and to compare the results with the performance of standard grouted anchors. Strength-only anchors represent the upper limit for the strength capacity of the device, when assuming that failure occurs in the steel or grouted element rather than in the masonry. This assumption re-

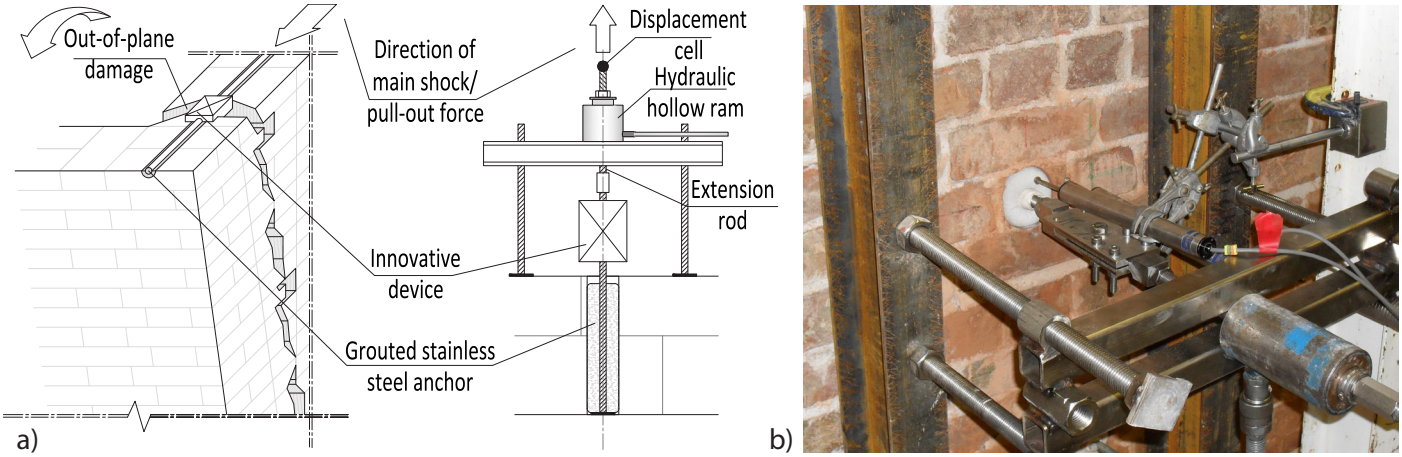

Figure 10. a) On-site and laboratory layout of dissipative anchoring devices in series with cross-tie, and b) set-up of frictional dissipative device pull-out test

Recycled Victorian bricks (220x110x70 mm) with 20 vertical holes		
Compressive strength	27.3 (CoV 19%)	[MPa]
NHL 5 lime mortar		
Mix proportions lime to sand	1:2	b.v
Flexural strength	0.3 (CoV 29%)	[MPa]
Compressive strength	1.0 (CoV 13%)	[MPa]
Masonry panels (1.4x0.35 m, 1.5 m high) English bond		
Compressive strength	6.7 (CoV 1%)	[MPa]
Bond strength (by wrench test)	0.67 (CoV 15%)	[MPa]

Table 3. Characterisation of specimen materials

sponds to criteria of safety of the anchorage (ductile failure), as well as to criteria of protection and preservation of the historic material.

The grouted anchor technology developed and distributed by Cintec International Ltd. is used: anchorage plates are not necessary as the anchorage force is transferred to the masonry by a shear mechanism rather than a bearing mechanism. The test set-up reproduces the portion of a tie anchored into a wall subject to seismic out-of-plane acceleration by way of a grouted socket. The pulling action of the testing apparatus represents the reaction of the anchor laying parallel to the main shock direction to the thrust of the overturning wall. The dissipative devices are to be positioned at the interface between the two orthogonal walls (Figure 10).

Following the prescriptions of BS EN 846-2 for the testing of ancillary components for masonry, five anchors per type were embedded in masonry panels undergoing a vertical load apt to simulate the typical compression perpendicular to bed joints throughout testing (0.05 and 0.1 MPa). Characterisation of materials is carried out according to relevant Eurocodes (BS EN 772 – masonry units, BS EN 1015 – mortar, BS EN 1052 – masonry); results are summarised in Table 3. Anchors are made of threaded M16 bar, AISI 304 stainless steel (EN no. 1.4301) class 70 (yield proof stress 300 MPa, ultimate tensile strength 700 MPa), 400 mm long, with a 60 mm diameter end plate and a 350 mm long fabric sleeve for grouting, and are installed in 80 mm diameter drilling holes passing through the wall. During tests, relative displacements at the outer surface of the grouted sleeve and brickwork are measured by transducers, while the global displacement is measured by a dial gauge positioned in series with the pulling apparatus, as shown in Figure 10.

For the testing set-up described above, failure in strength-only anchors may occur: 1) at the bond between the steel profile and the grout (1a), between the grouted element and the parent material (1b), or between adjoining bricks (1c), 2) by tensile failure in the masonry units, or 3) by a mixed mode including any of the others. Tests aimed to prove that these types of damage can be prevented thanks to the dissipative anchoring devices, which were designed to yield or activate the friction mechanism before cracking in the parent material.

For strength-only anchors, failure at the bond between the grouted sleeve and the parent material is the main mode of failure and the first to occur, then followed in some cases by a further increase in stiffness and cracking to other elements of the assembly (Figure 11). Accidental crushing of masonry at the support of the pulling apparatus can also occur due to the test set-up (failure type No 4).

The values of pull-out force measured experimentally can be compared to design values calculated on the basis of the material properties and the expected mode of failure. According to more extensive tests results reported in Zhou et al. (2008), the bond strength measured by wrench test correlates to a value of characteristic initial shear strength f_{vk0} equal to 0.42 MPa. Thus, characteristic shear strength

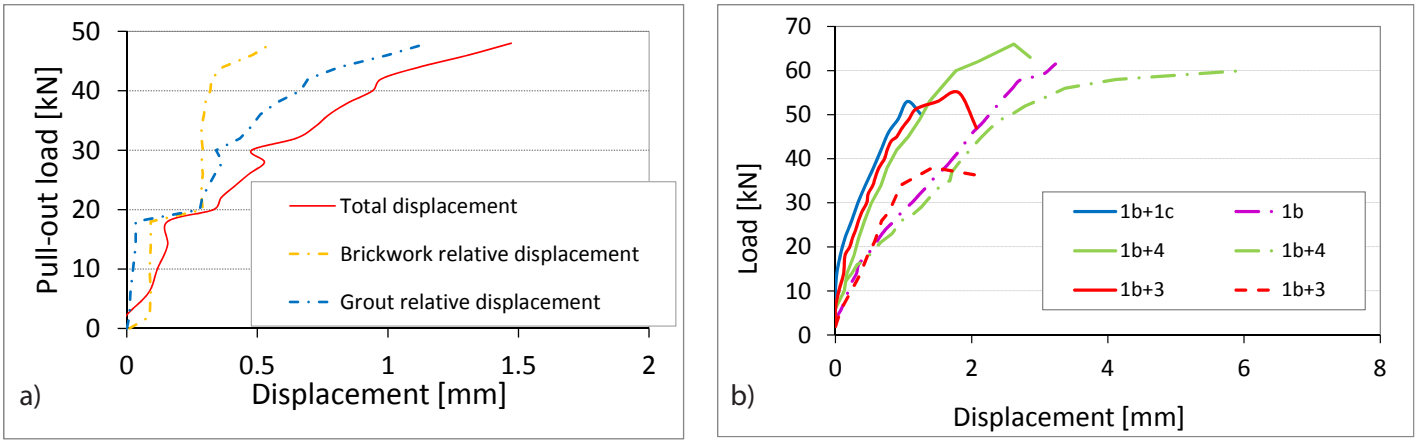

Figure 11. a) Relative displacements within assembly of strength-only anchor showing that failure in the bond between grouted sleeve and parent material is prevalent; b) load-displacement graph for tested strength-only anchors.

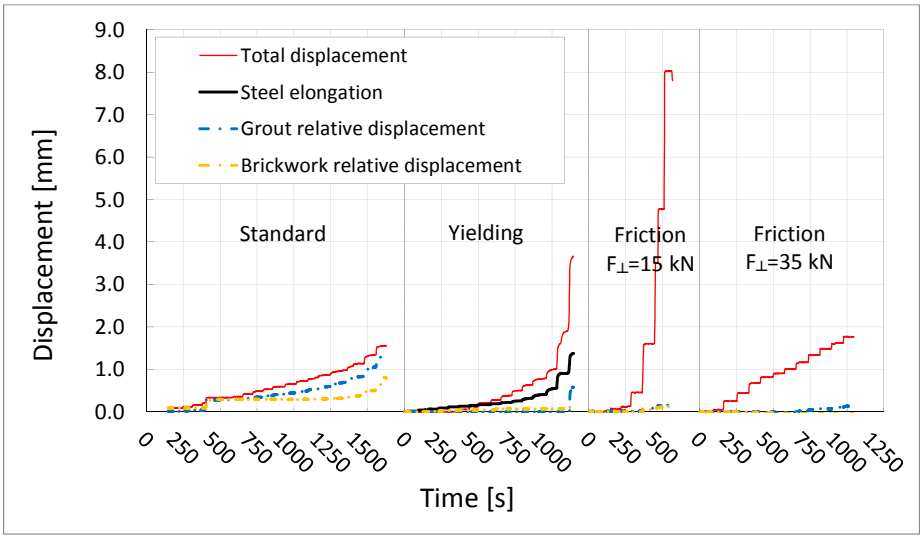

Figure 12. Relative displacements in a standard anchor and in anchors in series with a yielding device or a friction device calibrated with two different levels of slip load.

is equal to (BS EN 1996-1-1: 2005):

$$f_{vk} = f_{vk0} + 0.4\sigma_d = 0.45/0.56 \text{ MPa} \qquad (5)$$

where σ_d is the compressive strength perpendicular to bed.

Therefore, considering the cylindrical failure surface of the grouted sleeve the pull-out capacity would be expected to be equal to 34/50 kN. However, while some of the strength-only anchors do achieve the higher target level of load, others fail below the lower bound, as it can be seen from the early change in stiffness in the load-deflection curves (Figure 11b). Although a ductile behaviour is displayed by anchors with lower capacity, the scattering of results indicates a problem in predicting and achieving a repeatable performance of this type of anchors. Furthermore, the ductile behaviour always involved damage in the substratum.

Conversely, yielding and frictional anchors achieve larger displacements with reduced or no damage to the substratum, as it can be observed from the comparison of the relative displacements occurring in the assemblies.

Cyclic dynamic pull-out tests

Standard pull-out tests, although useful to compare the performance of dissipative and strength-only anchors embedded in low shear masonry, have one limit: only a portion of a structural connection rather than the whole corner is modelled. Furthermore, tests were performed in a monotonic regime so that the progressive deterioration of materials due to repeated loading was not taken into account.

Therefore, cyclic dynamic pull-out tests were designed and carried out. Specimens model the T-joint between two perpendicular walls connected by a passing anchor: one wall simulates the wall parallel to the main shock direction and is therefore restrained to the laboratory strong wall by means of the anchor; the other wall undergoes out-of-plane horizontal loading. The test set-up is devised including details such as a smaller overlapping of bricks at the joint between the two walls and the presence of a hinge at the base of the horizontally loaded wall so as to achieve an overturning mechanism whereby the horizontal load is transmitted from the front wall to anchor. The resisting action that arises at the end of the anchor fixed to the strong wall represents the resisting action of the portion of anchor embedded in a wall.

Three anchors per type were embedded in the T-shaped masonry panels, which are also undergoing a vertical load

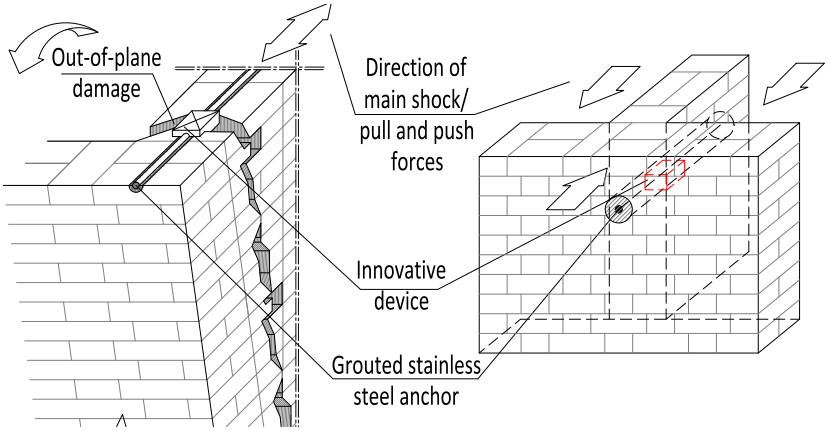

a)

b)

Figure 13. a) On-site and laboratory layout of dissipative anchoring devices in series with cross-tie, and b) set-up of cyclic dynamic pull-out test.

Recycled handcut solid bricks (220x110x70 mm)		
Compressive strength	12.8 (CoV 14%)	[MPa]
NHL 5 lime mortar		
Mix proportions lime to sand	1:2	b.v
Flexural strength	0.2 (CoV 19%)	[MPa]
Compressive strength	0.5 (CoV 25%)	[MPa]
T-shaped masonry wallets, double bond		
Compressive strength	3.1 (CoV 16%)	[MPa]
Bond strength (by wrench test)	0.33 (CoV 20%)	[MPa]

Table 4. Characterisation of specimen materials.

apt to simulate the typical compression perpendicular to bed joints throughout testing (0.05 and 0.1 MPa).

Characterisation of materials is carried out according to relevant Eurocodes (BS EN 772 – masonry units, BS EN 1015 – mortar, BS EN 1052 – masonry); results are summarised in Table 4. Anchors are made of threaded M16 bar, AISI 304 stainless steel (UNI 14301) class 70 (yield proof stress 300 MPa, ultimate tensile strength 700 MPa) and are installed in 80 mm diameter drilling holes.

During tests, relative displacements at the outer surface of the grouted sleeve and brickwork are measured by transducers placed at various levels, while cyclic loads are measured by load gauges positioned in series with the push and pull jacks. The amplitude of cycles is maintained constant for three cycles and then increased.

For the test set-up described above, failure was expected to occur initially by diagonal in-plane cracking of the restrained wall and eventually by failure of the head of the anchorage according to one of the failure modes described in the previous section. Conversely, in the case of dissipative devices, only a vertical crack at the joints between the two walls was expected to open, whereas the controlled displacement provided by the anchors was expected to prevent other damage to occur in the parent material.

However, due to the extremely low mechanical properties of materials, the bond between the grouted sleeve of the strength-only anchor in the front walls and the parent material fail at very early stages of tests; because of this early failure, load is not transmitted to the rear wall by the anchor and in-plane cracking doesn't occur (Figure 14). On the contrary, in the case of anchors in series with the dissipative devices, in-plane cracking appears as consequence of the effective connection. Whilst the yielding threshold of the hysteretic anchors is still too high to avoid the final pull out of the head of the anchorage, the frictional devices are able to provide the required level of relative displacement throughout testing, since the level of activation of slippage within the device can be controlled and modified (Figure 15).

Numerical simulation

A set of FE models developed using the Algor© commercial package is used to investigate the behaviour of the dissipative elements of both dissipative anchoring devices.

Since tests proved that the post-elastic behaviour of the lower capacity steel is predominant within the yielding anchor, the first three-dimensional model reproduces the hysteretic element without accounting for either the grouted anchor or the brickwork; therefore, one end of the device is fully constrained and the other is subjected to increasing positive load. The behaviour of steel (stainless steel 304, class 50) is modelled using a von Mises stress-strain curve derived by the application of the Ramberg-Osgood model, as modified by Rasmussen (2003) and encompassed by Eurocode 3. Standard material parameters for the applied type of steel are used (Table 5).

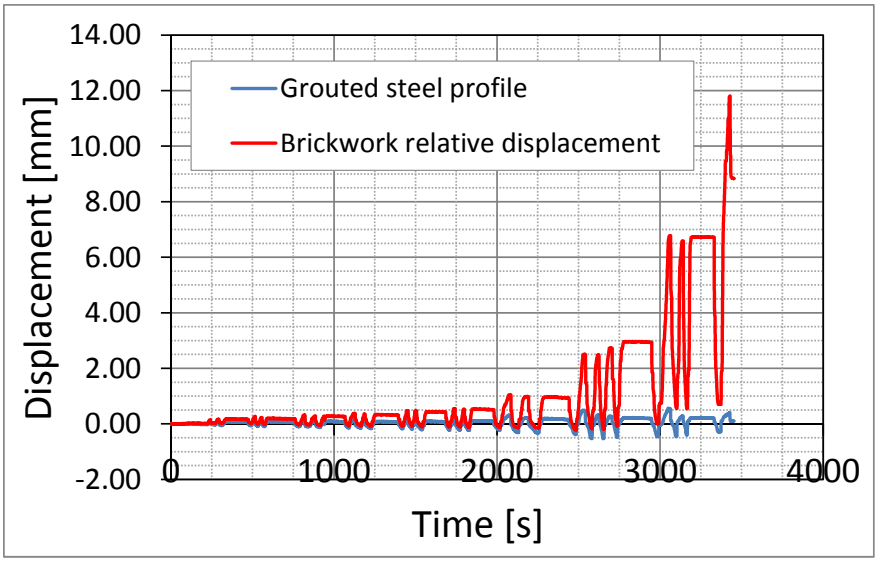

Figure 14. Premature failure of the bond between grouted sleeve and parent material T-shaped wallets strengthened by strength-only anchors.

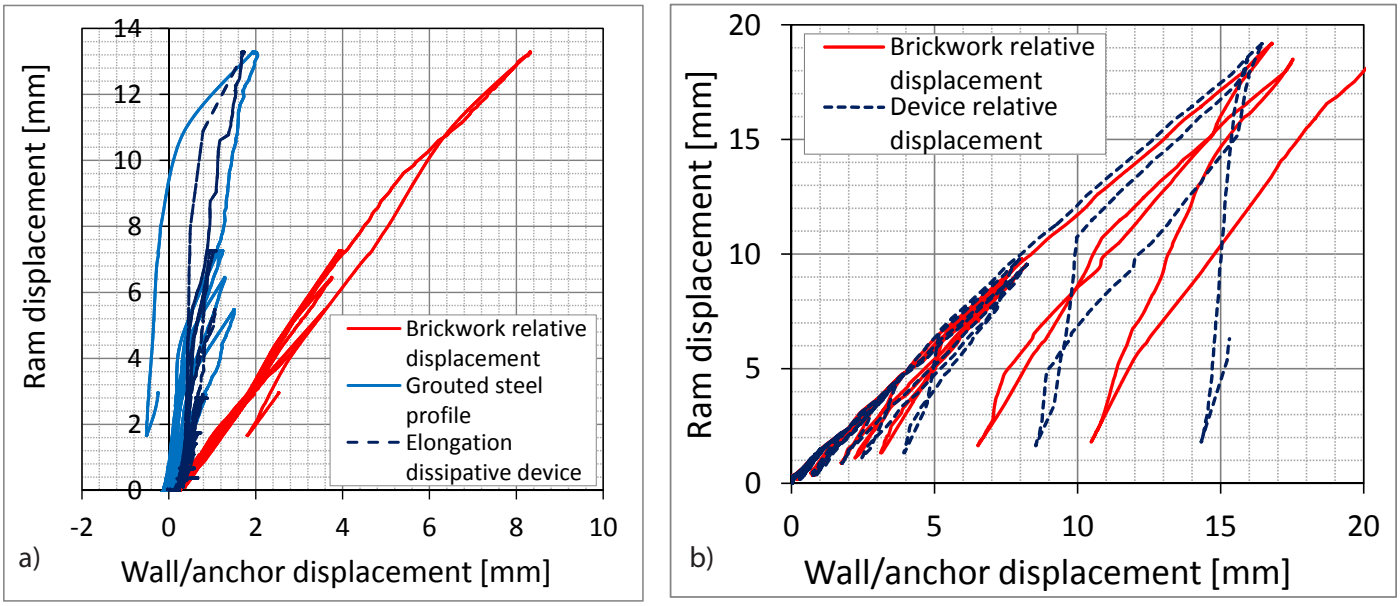

Figure 15. Load deflection curves of T-shaped walls strengthened by a) yielding device and b) frictional device. Whereas the total displacement of the front wall is achieved through the relative motion within the frictional device, the yielding device is not yet in its plastic range when the bond in the front wall fails.

Although the post-elastic branch of the load-deflection curves derived from tests and the FE model have a similar shape, the transition from the elastic to the non-linear range in the model occurs for higher values of force; moreover the experimental graph features lower stiffness due to the presence of the grouted element and brickwork, which are not considered in the model (Figure 16), but proved influential in matching computational and experimental results.

Hence, a two-dimensional model was developed accounting for the presence of grout and brickwork. In order to improve the computational performance of the model, only the dissipative element (stainless steel class 50) and the grouted part of the anchor (stainless steel class 70) are defined by a non-linear model with kinematic hardening, while the other materials are considered elastic; the output of the characterisation tests and the producer specifications are used for mechanical properties (Table 5). The assumption of linear behaviour for the grout and parent material is justified by the fact that negligible deformations were recorded during tests. Anchor and grout are considered bonded, as no failure at the interface between steel and grouted socket was observed; the bond between the grout and the parent materials is instead modelled by a surface-to-surface contact, applying a coefficient of friction so as to simulate the shear strength at the interface. Better agreement with experimental curves is obtained (Figure 17).

A set of two FE models was also developed using the Algor© commercial package to investigate the behaviour of the two versions of stick-slip tie that had been developed within the framework of the KTP project. Two-dimensional models are used so as to optimise the computational

	Stainless steel 304		Grout	Brickwork
	Class 50	Class 70		
Yield strength [MPa]	300	450	-	-
Ultimate strength [MPa]	500	700	-	-
Young's modulus [Gpa]	193	193	20.7	2.76
Poisson coefficient [-]	0.28	0.28	0.15	0.2

Table 5. Mechanical properties of materials used in the FE models.

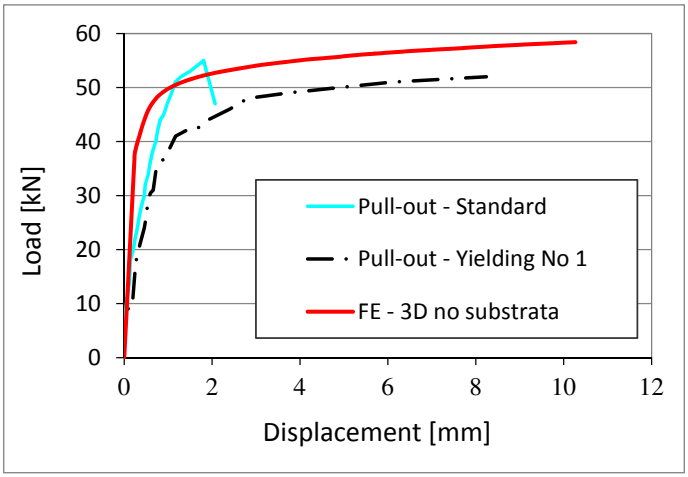

Figure 16. Monotonic increasing load - comparison pull-outs and FEs of isolated device.

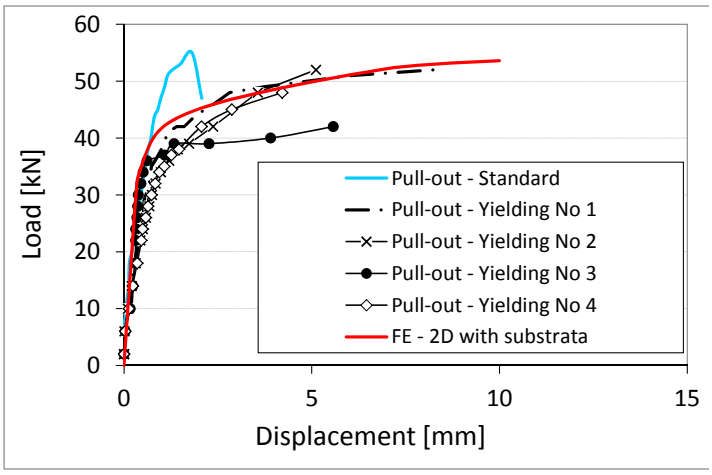

Figure 17. Monotonic increasing load - comparison pull-outs and FEs of device embedded in substrata.

time, and the behaviour of steel is simulated by a perfectly elastic model since inelastic deformations are not expected to occur in any of the pieces of the assembly for the applied levels of load; such assumption is based on the results of strain measurements collected during previous campaigns of tests (Paganoni and D'Ayala, 2009). Initially, devices are reproduced without accounting for either the portion of grouted anchor or the brickwork in order to calibrate the mechanical parameters, and in particular the coefficient of friction, by comparison with experimental data.

Standard material parameters are used for the stainless steel AISI 304 (EN no. 1.4301) class 50 (see Table 5), whilst the value of the static coefficient of friction is varied, assuming values ranging between 0.25 and 0.4. The contact among sliding steel elements is modelled as surface to surface contact. Two sets of forces are applied to the models: the perpendicular load and the load along the axis of the anchor. Simulations are undertaken for different values of orthogonal force, with pulling load linearly increasing.

Models are able to reproduce fairly well the load-deflection curves determined experimentally for the first version of the prototype by cyclic pseudo-static tests (Figure 18), and for the second version via pull-out tests (Figure 19). A friction coefficient equal to 0.3 is chosen as best match between FE, this confirming experimental results too, although the FE model remains consistent with the Coulomb formulation and, therefore, is not able to recreate the effects of the geometric imperfections that determine the mechanical locking, which can be seen affecting the device for higher levels of orthogonal load (e.g. F = 31.5 kN).

It is worth noticing that, although in the first version of the device such stick-and-slip behaviour is not detectable, the prototype was sensitive to misalignments and out-of-plane motions within the assembly; the design of the second version of the device overcomes these issues and has therefore a better performance, notwithstanding the need for further fine tuning. The second version of the friction prototype is also modelled when embedded in the parent material, following the same approach as for the yielding device, to investigate the influence of the strength of bond and parent materials on the performance of the device. The change in stiffness in the linear branch of the load-deflection curve is hardly detectable (Figure 20); prior to the activation of the friction mechanism, loads are too low to affect the substrata, unless micro-cracking occurs (e.g. experimental curve No. 2), but this effect was not included in the model. Furthermore, as it can be observed in Figure 21, stresses in the parent material for the highest values of slip and perpendicular loads are negligible, accordingly to the conclusions drawn from the output from tests. The portion of stainless steel bar joining the friction device to the grouted socket is also far from values of yielding (75 MPa against f_y = 450 MPa).

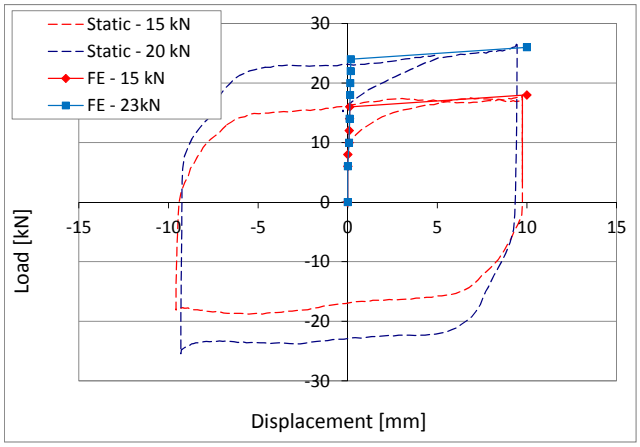

Figure 18. Friction device, version 1 – comparison FE and cyclic tests on isolated device.

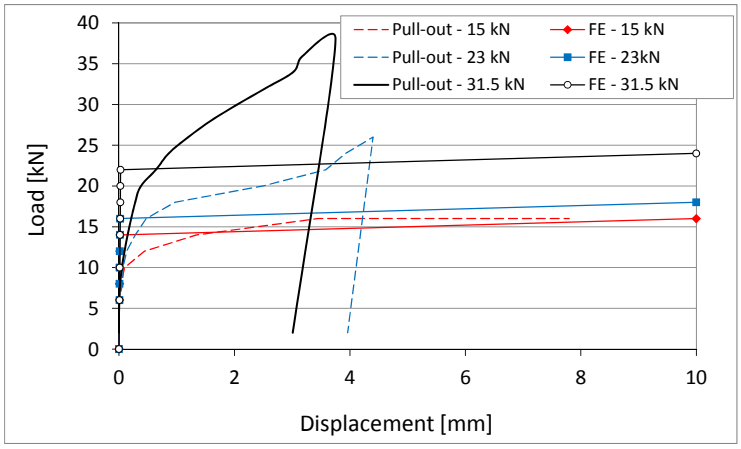

Figure 19. Friction device, version 2 - comparison FE and pull-out tests.

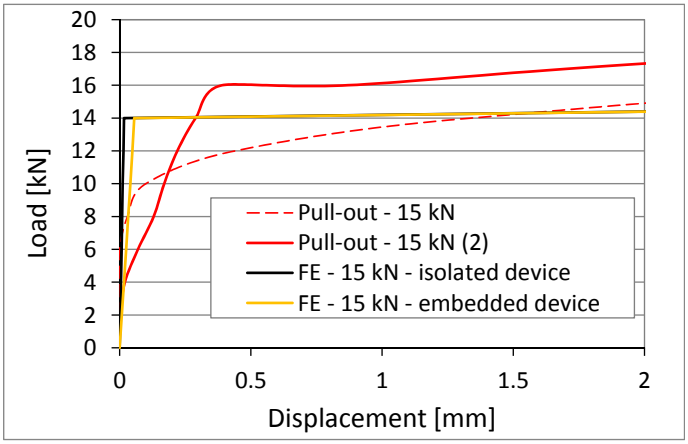

Figure 20. Comparison experimental and FEs with and without substrata (detail).

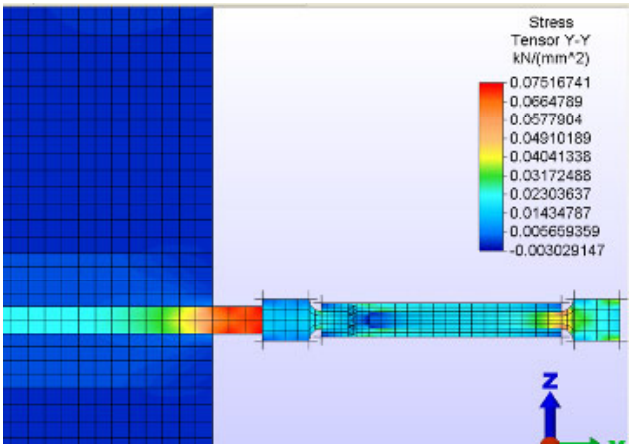

Figure 21. Longitudinal stress at connection between friction device and grouted anchor (detail).

Conclusions

A limit state analysis of a sample of buildings in the historic city centre of L'Aquila has been conducted with the aim of assessing their seismic capacity and defining their damage patterns. The definition of capacity curves and performance points allows an assessment of the historic building stock using the same methodology and parameters as for modern engineered structures. The derivation of fragility curves in terms of lateral displacement is useful to extend the results to the rest of the building stock and to quantify and prioritise intervention in relation to expected seismic risk. The FaMIVE procedure shows good agreement in terms of both predicted levels of vulnerability and predicted collapse mechanisms, indicating that the correct simulation of connections and boundary constraints for the facades is a necessary but also sufficient condition to predict their failure behaviour with a limit state analysis. The evaluation of the correct collapse state is highly sensitive to the level of ductility assumed. The use of values typically recommended in codes of practice leads to overestimates of damage.

Experimental results show that frictional anchors provide controlled movement and reduce the load transmitted to the parent material so that, in the case of a poor quality substratum premature bond failure of the anchorage is prevented despite in-plane cracking and in case of good quality masonry any damage in the substratum is avoided. Yielding devices perform well in good quality substrata, but for low shear capacity masonry, restriction of the dimensions of the devices itself mean that the anchorage cannot yield and displace for the required level of load.

A set of Finite Element models was developed and calibrated with experimental data through monotonic linear and non-linear analysis, showing good agreement and confirming the values derived for mechanical parameters such as the coefficient of friction. For high levels of perpendicular forces, the FE model of the friction device conserved a behaviour consistent with the Coulomb friction, this representing the target performance of the prototypes. The influence of the parent material was investigated by modelling both isolated devices and devices embedded in a parent material; while a difference can be observed for hys-

teretic devices, the change in stiffness of the overall load-deflection curve of friction devices is hardly detectable. Models confirmed that deformations in the parent material and in the joint with the grouted part of the anchor are negligible, as observed from experimental results.

In conclusion, the frictional anchor device was able to reach a displacement comparable with prescribed inter-storey drifts and prevent pull-out failure; it is therefore consistent from a point of view of performance design, although the assembly will need additional refinements and further tests will be required to validate the dynamic behaviour of the assembly in masonry panels.

References

Benedetti D. (2004). Increasing Available Ductility in Masonry Buildings via Energy Absorbers. Shaking Table Tests. *European Earthquake Engineering*, N. 3/2004.

Bernardini A. & Lagomarsino S. (2008). The Seismic Vulnerability of Architectural Heritage. In *Proc. of the Institution of Civil Engineers - Structures and Buildings*, **161**(SB4): 171–181.

BS EN 772:2000 – *Methods of Test for Masonry Units*, 2000.

BS EN 846-2:2000 – *Methods of Test for Ancillary Components for Masonry, Part 2: Determination of Bond Strength of Prefabricated Bed Joint Reinforcement in Mortar Joints*, 2000.

BS EN 1015:1999 – *Methods of Test for Mortar for Masonry,* 1999.

BS EN 1052:1999 – *Methods of Test for Masonry*, 1999.

BS EN 1996-1-1:2005. Eurocode 6 – *Design of Masonry Structures*, 2005.

Casapulla, C. & D'Ayala, D. F. (2006). In-plane Collapse Behaviour of Masonry Walls with Frictional Resistance and Openings. In *Proc. Structural Analysis of Historical Construction*, Delhi, India, Nov 2006.

Crowley H., Pinho R. & Bommer J.J. (2004). A Probabilistic Displacement-Based Vulnerability Assessment Procedure for Earthquake Loss Estimation. *Bulletin of Earthquake Engineering*, **2**(2):173-219.

D'Ayala, D., Paganoni, S. (2011). Assessment and Analysis of Damage in L'Aquila Historic City Centre after 6th April 2009. *Bulletin of Earthquake Engineering*, **9**(1): 81-104.

D'Ayala, D. (2008). Seismic Vulnerability and Risk Assessment of Cultural Heritage Buildings in Istanbul, Turkey. In *Proc. of 14th World Conference on Earthquake Engineering*, Beijing, China, Oct 2008.

D'Ayala, D. (2005). Force and Displacement Based Vulnerability Assessment for Traditional Buildings. *Bulletin of Earthquake Engineering*, **3**(3):235-265.

D'Ayala, D & Ansal, A. (2009). Non-linear Push-Over Assessment of Historic Buildings in Istanbul to Define Vulnerability Functions. In *Proc. WCCE – ECCE – TCCE Joint Conference: Earthquake and Tsunami*, Istanbul, Turkey, June 2009.

D'Ayala, D. & Speranza, E. (2003). Definition of Collapse Mechanisms and Seismic Vulnerability of Historic Masonry Buildings. *Earthquake Spectra*, **19**(3):479-509.

D'Ayala D. & Speranza E. (2002). An Integrated Procedure for the Assessment of Seismic Vulnerability of Historic Buildings. In *Proc. of 12th European Conference of Earthquake Engineering*, Paper Reference 561. Elsevier Science Limited, London.

EN 1998 Eurocode 8 – *Design of Structures for Earthquake Resistance*, 1998.

Indirli, M. & Castellano, M. G. (2008). Shape Memory Alloy Device for the Structural Improvement of Masonry Heritage Structures. *International Journal of Architectural Heritage*, **2**: 93-119.

Italian Ministry of Cultural Heritage and Activities (2006). *Guidelines for Evaluation and Mitigation of Seismic Risk to Cultural Heritage.*

Lagomarsino S. & Giovinazzi S. (2006). Macroseismic and Mechanical Models for the Vulnerability and Damage Assessment of Current Buildings. *Bulletin of Earthquake Engineering*, **4**(4):415-443.

Lang, K. & Bachmann, H. (2004). On the Seismic Vulnerability of Existing Buildings: a Case Study of the City of Basel. *Earthquake Spectra*, **20**(1):43-66.

Mandara, A. & Mazzolani, F.M. (1994). Seismic Upgrading of Churches by Means of Dissipative Devices. In *Proc. STESSA: Behaviour of Steel Structures in Seismic Areas.*

OPCM, no. 3431, May 3, 2005. Official Bulletin no. 107, May 10, 2005 (in Italian). Gazzetta Ufficiale - Serie Generale n. 105 (Suppl. Ordinario n. 72).

Paganoni, S. & D'Ayala, D. (2009). Development and Testing of Dissipative Anchor Devices for the Seismic Protection of Heritage Buildings. In *Proc. ANCER Workshop 2009*, Urbana-Champaign, ILL, USA, Aug 2009.

Rasmussen, K. JR (2003). Full-range Stress-strain Curves for Stainless Steel Alloys. *Journal of Constructional Steel Research*, **59**(1):47-61

Tomaževič, M. (1999). *Earthquake-resistant Design of Masonry Buildings*. A. S. Elnashai & P. J. Dowling Ed., London, UK: Imperial College Press.

Zhou, Z., Walker, P. & D'Ayala, D. (2008). Strength Characteristics of Hydraulic Lime Mortared Brickwork. In *Proc. of the Institution of Civil Engineering – Construction Materials*, **161**(4):139-146.

Brian Baptie, from the British Geological Survey in Edinburgh, puts recent events in Japan into a British perspective.

Could it happen here?

Could a magnitude 9 earthquake and tsunami like the one that struck Japan affect the British Isles? The short answer is no. Huge mega-thrust earthquakes like this only happen at plate boundary subduction zones where one of the Earth's tectonic plates is being pushed down, or subducted, beneath another. Places where this happens include Japan, Sumatra and South America all of which have had earthquakes of magnitude 8.5 or greater in the last few years that have resulted in tsunami. The British Isles sits in the middle of a tectonic plate, Eurasia. Our nearest plate boundary is at the mid-Atlantic ridge, where the earthquakes are too small to generate tsunami. The nearest subduction zones to Britain lie at the Hellenic Arc, south of Greece and in the Caribbean. Tsunami have occurred in both these regions in historic times, but did not affect the UK. The largest recorded British earthquake had a magnitude of 5.8 (6.1 ML) and was over 65,000 times smaller than the Tohoku earthquake in Japan (Musson, 1994). Although it occurred under the North Sea it was too small to generate a tsunami. This event is close to the maximum credible magnitude for a British earthquake. The UK experiences a magnitude 5 earthquake roughly every 10-20 years. These events typically cause some superficial damage.

In contrast, the Tohoku earthquake of 11 March 2011 (Simons et al., 2011) ruptured a 400 km long segment of the plate boundary that lies east of Japan, running from the northern end of Honshu roughly south almost as far as Tokyo. East of Honshu, the Pacific plate is moving west at around 8 cm/year and is being pushed down, or subducted, underneath Japan at the Japan Trench. The plates had been locked together for many years before enough strain accumulated to allow the fault to rupture. The average amount of slip on the fault was around 8 m, resulting in Japan moving several metres east during the earthquake. Coseismic slip exceeded 50 m in places. This motion resulted in over 3 metres of uplift of the seafloor along the fault (Sato et al., 2011), displacing huge volumes of water and causing the giant waves or tsunami that spread out from the epicentre like ripples on a pond. The first wave took around thirty minutes to reach the coast of Japan as was followed by a number of other waves, which surged several kilometres inland.

However, it may surprise many people to learn that tsunami have occurred in Britain in the past.

Over 7000 years ago, a massive submarine slide off the coast of Norway, known as the Storegga slide (Bondevik et al., 1997), resulted in a tsunami reaching the northeast coast of Britain. Evidence of this can be found in geological deposits from northeast England to north of the Arctic

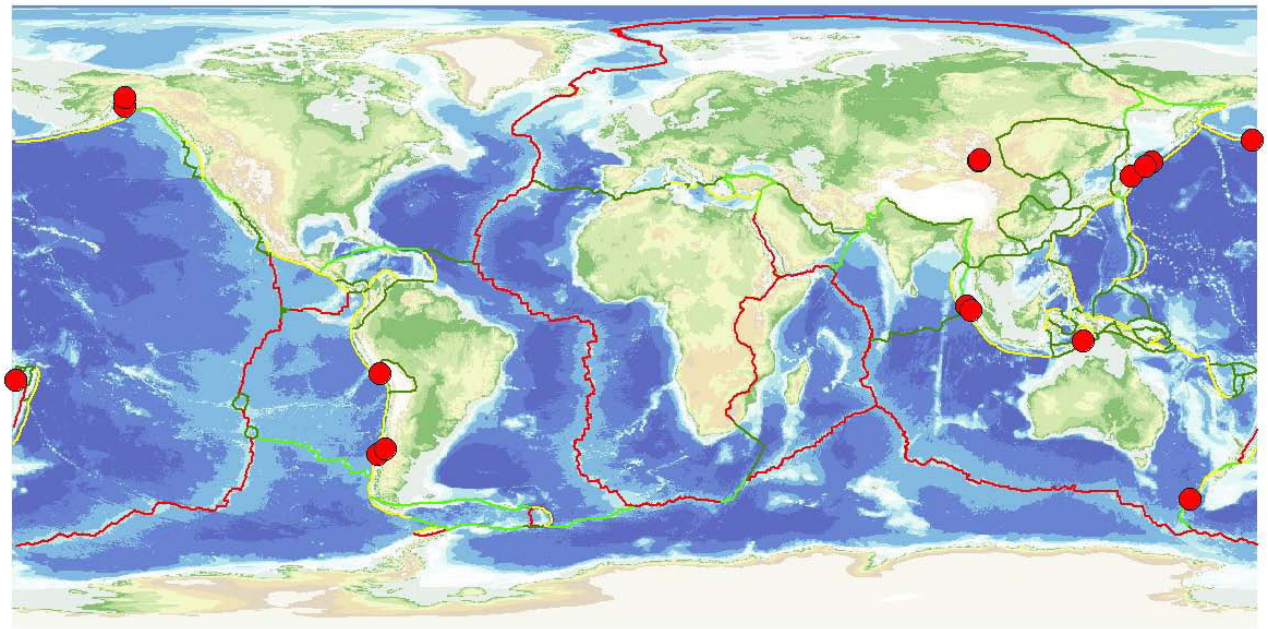

Figure 1. Earthquakes greater than magnitude 8.2 (red circles). These tend to cluster at plate boundary subduction zones (yellow lines). By contrast there are no great earthquakes at mid-ocean ridges (red lines) such as the Mid-Atlantic ridge.

Circle. These show that the wave reached over 20 m above sea level at Sullom Voe, Shetland. However this quickly decreases to the south with 3-4 m in northeast Scotland and 1 m in northeast England. A repeat of this event is unlikely, since geological models suggest that another Ice Age is needed to re-establish the conditions for a similar failure.

In 1755, Lisbon was destroyed by a magnitude 8+ earthquake and tsunami. The tsunami reached the southwest coast of England and its arrival in Mount's Bay, Cornwall was observed by the naturalist William Borlase (1755), who described several large waves crashing against the shore over a period of two hours. A study by BGS, HR Wallingford and the Proudman Oceanographic Laboratory commissioned by Defra looked in detail at the possible effects of another earthquake like the 1755 Lisbon earthquake (Richardson et al., 2006). Modelling results suggest that the wave would take around 5 hours to reach Britain, with maximum wave heights of 1-2 m around the majority of Cornwall. Such wave heights are similar to those resulting from typical storm surges that are experienced on a far more frequent basis.

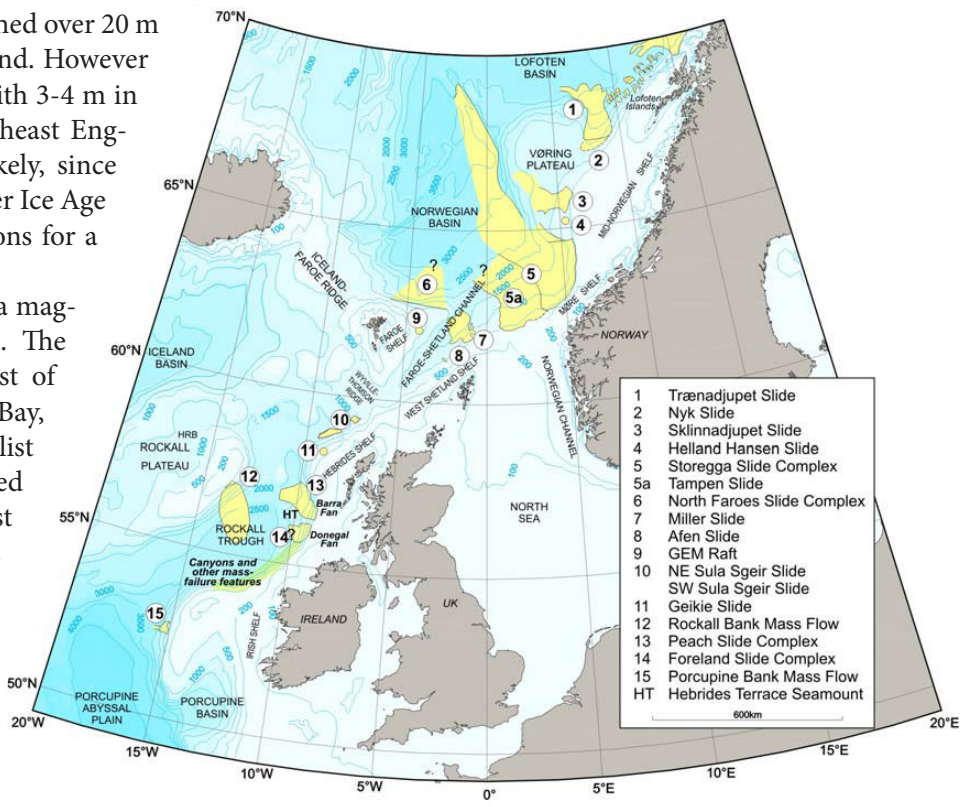

Figure 2. Slides on the NW European continental margin.

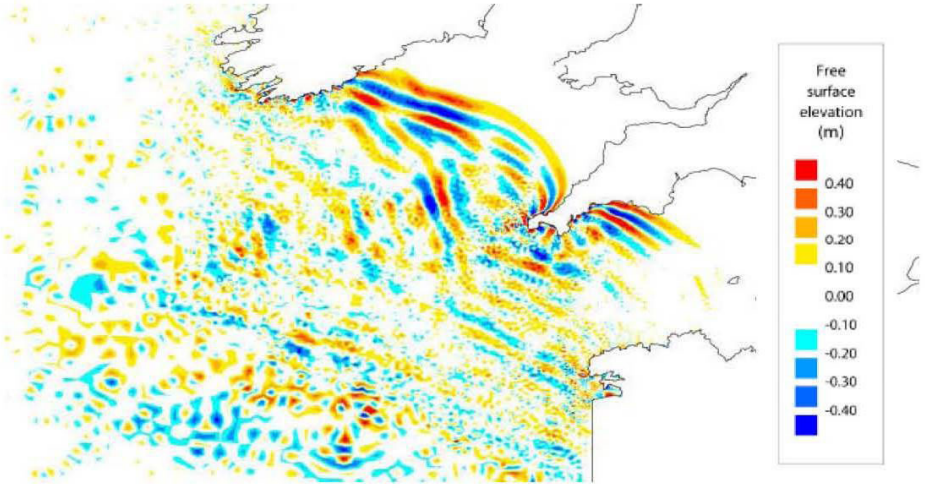

Figure 3. Modelled free surface elevation of the sea surface 5 hours after a magnitude 8.7 earthquake displaces the sea-bed in the area of the Gorringe Bank, west of Lisbon.

References

Bondevik, S. Svendsen, J.I. Johnsen, G. Mangerud J. & Kaland, P.E. (1997). The Storegga tsunami along the Norwegian coast, its age and run-up, *Boreas*, **26**, 29–53.

Borlase, W. (1755). Letter to the Rev Charles Lytteton. *Philosophical Transactions of the Royal Society of London*, **49**: 373-378

Musson, R.M.W. (1994). *A catalogue of British earthquakes*, British Geological Survey, Technical Report WL/94/04.

Richardson et al. (2006). *Tsunamis – Assessing the Hazard for the UK and Irish Coasts*, Study commissioned by Defra Flood Management, http://www.defra.gov.uk/environment/flooding/risk/tsunami.htm

Sato et al. (2011). Displacement Above the Hypocenter of the 2011 Tohoku-Oki Earthquake, *Science*, DOI: 10.1126/science.1207401

Simons et al. (2011). The 2011 Magnitude 9.0 Tohoku-Oki Earthquake: Mosaicking the Megathrust from Seconds to Centuries, *Science,* DOI: 10.1126/science.1206731

Notable Earthquakes: January - March 2011.

Reported by British Geological Survey

Issued by: Davie Galloway, British Geological Survey, June 2011.
Non British Earthquake Data supplied by The United States Geological Survey.

Year	Day	Mon	Time UTC	Lat	Lon	Dep km	Magnitude ML	Mb	Mw	Location
2011	01	JAN	09:56	26.80S	63.08W	577			7.0	ARGENTINA
2011	02	JAN	20:20	38.31S	73.27W	24			7.1	ARAUCANIA, CHILE
2011	03	JAN	21:03 09s	54.17N	1.65W	7	3.6			RIPON, N YORKSHIRE
Felt throughout Yorkshire and also felt in Lancashire, Cumbria, Greater Manchester, Durham and Tyne & Wear with a maximum intensity of 5 EMS.										
2011	03	JAN	21:03 29s	54.17N	1.65W	7	2.6			RIPON, N YORKSHIRE
Felt North Yorkshire (3 EMS).										
2011	09	JAN	10:03	19.16S	168.31E	24			6.6	VANUATU
2011	12	JAN	21:32	26.96N	140.00E	524			6.5	BONIN ISLANDS, JAPAN
2011	13	JAN	16:16	20.62S	168.46E	9			7.0	LOYALTY ISLANDS
2011	14	JAN	22:45	55.82N	6.33W	9	2.1			ISLAY, ARGYLL & BUTE
Felt Islay (3 EMS).										
2011	17	JAN	14:28	51.60N	3.59W	10	1.8			MAESTEG, BRIDGEND
2011	18	JAN	11:04	57.73N	4.57W	8	1.7			STRATHRANNOCH
2011	18	JAN	20:23	28.73N	63.93E	68			7.2	SOUTHWEST PAKISTAN
Two people killed, several injured and at least 200 homes damaged in Balochistan.										
2011	23	JAN	06:02	56.82N	5.78W	16	3.5			GLENUIG, HIGHLAND
Felt in Argyll & Bute and Highland regions with a maximum intensity of 4 EMS.										
2011	27	JAN	06:04	50.00N	1.91W	5	2.5			ENGLISH CHANNEL
2011	01	FEB	07:11	24.69N	97.93E	35		4.8		MYANMAR/CHINA BORDER
One person injured in Pingyuan and at least 700 houses damaged or destroyed and 80,000 people displaced in the Yianjiang area.										
2011	03	FEB	07:55	61.38N	3.59E	10	3.4			NORWEGIAN SEA
2011	10	FEB	14:39	4.18N	122.90E	546			6.5	CELEBES SEA
2011	10	FEB	14:41	4.02N	123.06E	532			6.6	CELEBES SEA
2011	11	FEB	20:05	36.40S	72.94W	26			6.8	OFFSHORE BIO-BIO, CHILE
2011	13	FEB	13:19	58.41N	1.97E	10	3.5			NORTHERN NORTH SEA
2011	14	FEB	03:40	35.38S	72.83W	21			6.6	OFFSHORE MAULE, CHILE
2011	21	FEB	10:57	26.14S	178.40E	557			6.6	FIJI ISLANDS REGION
2011	26	FEB	23:51	43.58S	172.68E	5			6.3	CHRISTCHURCH, NZ
181 people killed, over 1,500 others injured (of which 164 were serious) and thousands of buildings destroyed or damaged in the Christchurch / Lyttelton area.										
2011	26	FEB	04:30	61.93S	2.03E	37	3.6			NORWEGIAN SEA
2011	09	MAR	02:45	38.44N	142.84E	32			7.3	HONSHU, JAPAN
2011	10	MAR	04:58	24.72N	97.97E	23			5.5	MYANMAR/CHINA BORDER
At least 25 people killed, 250 injured, over 13,000 buildings destroyed or damaged and several roads damaged in the Pingyuan area, China.										

Year	Day	Mon	Time UTC	Lat	Lon	Dep km	Magnitude ML	Mb	Mw	Location
2011	11	MAR	05:46	38.32N	142.35E	32			9.0	HONSHU, JAPAN
At least 11,600 people killed and 16,450 still missing, over 170,500 people displaced and at least 155,000 homes and buildings destroyed or heavily damaged. Over 2,000 roads, 56 bridges and 36 railways also damaged or destroyed by the earthquake and resultant tsunami. A Pacific Ocean wide tsunami was generated.										
2011	11	MAR	06:08	38.97N	143.37E	33		6.7		HONSHU, JAPAN
2011	11	MAR	06:15	36.27N	141.14E	35			7.9	HONSHU, JAPAN
2011	11	MAR	06:18	36.02N	142.27E	16		6.6		HONSHU, JAPAN
2011	11	MAR	06:20	36.00N	142.07E	49		6.5		HONSHU, JAPAN
2011	11	MAR	06:25	38.06N	144.59E	18			7.7	HONSHU, JAPAN
2011	11	MAR	06:29	37.83N	144.21E	42		6.5		HONSHU, JAPAN
2011	11	MAR	08:19	36.16N	141.58E	12		6.5		HONSHU, JAPAN
2011	11	MAR	11:36	39.28N	142.52E	12		6.5		HONSHU, JAPAN
2011	12	MAR	01:47	37.59N	142.65E	20			6.5	HONSHU, JAPAN
2011	24	MAR	13:55	20.72N	99.82E	8			6.8	MYANMAR
At least 74 people killed, 111 injured and 413 buildings damaged in eastern Myanmar. A further one person was killed in northern Thailand and another 12 were injured, over 9,000 houses and several reservoirs and roads were damaged in Yunnan, China.										
2011	26	MAR	16:09	55.76N	5.72W	10	1.6			SOUND OF JURA
2011	29	MAR	11:13	57.40N	4.35W	7	2.4			INVERNESS, HIGHLAND
Felt Inverness (3 EMS).										
2011	29	MAR	23:21	55.78N	6.32W	8	1.3			ISLAY, ARGYLL & BUTE
Felt Islay (2-3 EMS).										

New Editor for the SECED Newsletter

After three years as Editor of the SECED Newsletter, Mr A Nielsen has indicated his willingness to stand down if and when a suitable replacement can be appointed. Anyone interested in taking over the reins should register his or her interest with the current Chairman of the Society, Professor Ahmed Elghazouli (a.elghazouli@imperial.ac.uk).

The successful applicant will be required to produce up to four Newsletters per year (depending on the volume of contributions), using an appropriate desktop publishing software package (Adobe InDesign will be supplied).

The benefits of the position include:

- A co-opted seat on the SECED Committee.
- Continuous Professional Development through service to a learned society.
- Lifetime honorary membership of SECED after minimum three years of service.
- Keeping up to date with the latest events, ideas and developments in the UK and abroad.

For further information regarding this position, please contact Andreas Nielsen (andreas.nielsen@jacobs.com).

Past and future events

There are no SECED evening meetings or other events planned for the summer. However, a number of events are in the pipeline for the forthcoming academic year (see table below). For access to past events, try visiting the SECED website where links to previous recorded events can be found. The recording of March's evening meeting, *Contributions of Field Case Histories to Geotechnical Earthquake Engineering*, presented by Prof I.M. Idriss of the University of California at Davis, is available for playback at the following link: http://ice.adobeconnect.com/p96679589/. The playback includes sight of the slides as part of the talk; however, if you wish to view the slides as a stand-alone file, these have been made available on the SECED website. Playbacks of some other recent SECED evening meetings are also available: *Non-Linear Soil-Structure Interaction* (Alain Pecker, November 2010): http://ice.emea.acrobat.com/p51719171/; *Earthquakes, Volcanoes & God* (David Chester, January 2011): http://ice.emea.acrobat.com/p73282097/.

Date	Event	Tentative title	Organisers
Sep 2011	Evening meeting	*Nuclear Facilities*	Chris Browitt (BGS)
Oct 2011	Evening meeting	*TK Hsieh Prize Talk: Lateral Pile Response in Liquefiable Soils*	Stavroula Kontoe (Imperial College)
Nov 2011	Evening meeting	*Capability of Faults*	Clark Fenton (Imperial College)

For up-to-date details of SECED events in 2011/2012, visit the website: **www.seced.org.uk**

SECED Newsletter

The SECED Newsletter is published quarterly. All contributions of relevance to the members of the Society are welcome. Manuscripts should be sent by email. Diagrams, pictures and text should be attached in separate electronic files. Hand-drawn diagrams should be scanned in high resolution so as to be suitable for digital reproduction. Photographs should likewise be submitted in high resolution. Colour images are welcome. Hard copy manuscripts are also welcome. Please contact the Editor of the Newsletter, Andreas Nielsen, for further details.

Email
andreas.nielsen@jacobs.com

Post
Editor SECED Newsletter
c/o The Secretary
SECED
Institution of Civil Engineers
One Great George Street
London, SW1P 3AA
United Kingdom

SECED

SECED, The Society for Earthquake and Civil Engineering Dynamics, is the UK national section of the International and European Associations for Earthquake Engineering and is an affiliated society of the Institution of Civil Engineers. It is also sponsored by the Institution of Mechanical Engineers, the Institution of Structural Engineers, and the Geological Society. The Society is also closely associated with the UK Earthquake Engineering Field Investigation Team. The objective of the Society is to promote co-operation in the advancement of knowledge in the fields of earthquake engineering and civil engineering dynamics including blast, impact and other vibration problems. For further information about SECED contact:

The Secretary
SECED
Institution of Civil Engineers
One Great George Street
London, SW1P 3AA, UK

Or visit the SECED website:
http://www.seced.org.uk